Modeling near-field radiative heat transfer from sharp objects using a general three-dimensional numerical scattering technique

Alexander P. McCauley,[1] M. T. Homer Reid,[1,2] Matthias Krüger,[1] and Steven G. Johnson[3]
[1]*Department of Physics, Massachusetts Institute of Technology, Cambridge, Massachusetts 02139, USA*
[2]*Research Laboratory of Electronics, Massachusetts Institute of Technology, Cambridge, Massachusetts 02139, USA*
[3]*Department of Mathematics, Massachusetts Institute of Technology, Cambridge, Massachusetts 02139, USA*
(Received 4 February 2012; published 4 April 2012)

We develop a general numerical method to calculate the nonequilibrium radiative heat transfer between a plate and compact objects of arbitrary shapes, making the first accurate theoretical predictions for the total heat transfer and the spatial heat flux profile for three-dimensional compact objects including corners or tips. In contrast to the known sphere-plate heat transfer, we find qualitatively different scaling laws for cylinders and cones at small separations, and, in contrast to a flat or slightly curved object, a sharp cone exhibits a local *minimum* in the spatially resolved heat flux directly below the tip. Our results may have important implications for near-field thermal writing and surface roughness.

DOI: 10.1103/PhysRevB.85.165104 PACS number(s): 44.40.+a, 02.70.Pt, 44.05.+e

I. INTRODUCTION

We make the first accurate theoretical predictions for near-field thermal transfer from three-dimensional (3D) compact objects of arbitrary shapes (including corners or tips) to a dielectric substrate. Our work is motivated by studies of noncontact thermal writing with a hot, sharp object[1,2] as well as recent experiments in near-field thermal transfer for spheres and plates.[3,4] These experiments have confirmed the theoretical predictions[5,6] that radiative heat transfer between two bodies at different temperatures is greatly enhanced as their separation is reduced to submicron scales, due to contributions from evanescent waves. This promises interesting new nonequilibrium physics at submicron separations; however, until recently the only rigorous theoretical results for thermal transfer concerned parallel plates. In the past years rigorous theoretical predictions for sphere-sphere[7] and sphere-plate[8,9] geometries as well as general formalisms for planar structures[10] and arbitrary shapes[8,11] have been presented. However, taken by themselves these techniques are limited to objects for which the scattering matrices are known analytically (e.g., spheres and plates in three dimensions) and cannot be directly applied to, e.g., cones and (finite) cylinders. As an alternative, stochastic finite-difference time-domain methods have been used to examine heat transfer for periodic structures,[12] but this method is not computationally well suited for compact objects in three dimensions. Therefore, nothing is yet known about the effects of, e.g., sharp tips on radiative thermal transfer. In order to investigate these effects, we develop a method capable of handling arbitrary compact objects and apply it to nontrivial shapes. The first part of our method builds on the scattering-theory formulations of Refs. 8,10,11. Our formalism differs in several ways from previous methods, the most important of which is the use of a three-body detailed-balance argument (described below) and a cylindrical wave multipole basis, in which a novel Gaussian quadrature approach is used to discretize the scattering matrix. Unlike the usual spherical wave basis, this allows us to concentrate our resolution on the surfaces adjacent to the substrate. The second part of our method involves the use of a boundary-element method, in which the object is described by a generic surface mesh,[13] to numerically compute the scattering matrices of the compact object in the cylindrical wave basis. In addition to the previously known sphere-plate heat transfer, we study both cylinder-plate and cone-plate configurations (see the sketch in Fig. 1), for which no known analytic solution exists. Our results exhibit clear scaling laws for the total heat transfer that distinguish locally flat structures (e.g., cylinders and spheres) from locally sharp structures (cones). In addition, we study the spatial distribution of the heat flux over the substrate, a result that is of importance for the so-called "heat stamp" application.[14,15] Previous treatments of this subject have approximated the heating/writing element as either a point dipole[16] or a large sphere,[14] neither of which correctly represents the shape of a real hot tip (e.g., an atomic force microscope tip). Our results show that the heat flux pattern depends strongly on the shape of the tip. Cones in particular have a flux pattern exhibiting an unusual feature: a local *minimum* in the heat flux directly below the tip, which we can explain with a modified dipole picture.

II. METHOD

In our setup, an object A at (local) temperature T_A faces a dielectric plate P at temperature T_P, in an environment E that is also at temperature T_P. We use the framework of Rytov's theory,[17] in which all sources emit radiation independently. In contrast to previous studies, we aim at the *spatially* resolved heat flux and take into account the environmental temperature. Although this quantity is not symmetric in A and P (as is the total transfer),[7] we can still avoid the explicit calculation of the nontrivial radiation of A, employing detailed balance[18] for three objects: at every point in space, the full flux from A at temperature T_A must equal the flux from P and E at temperature T_A (with opposite signs), and we can completely describe the system with radiative sources from P and E only. To compute the power flux, we first compute the nonequilibrium electric-field correlator $\langle \mathbf{E}(\mathbf{x}) \otimes \mathbf{E}^*(\mathbf{x}') \rangle_j^{\text{neq}}$ due to radiation from $j = P, E$ for general $\mathbf{x} \neq \mathbf{x}'$; the total correlator contains an additional equilibrium contribution,[8,10,11] which does not

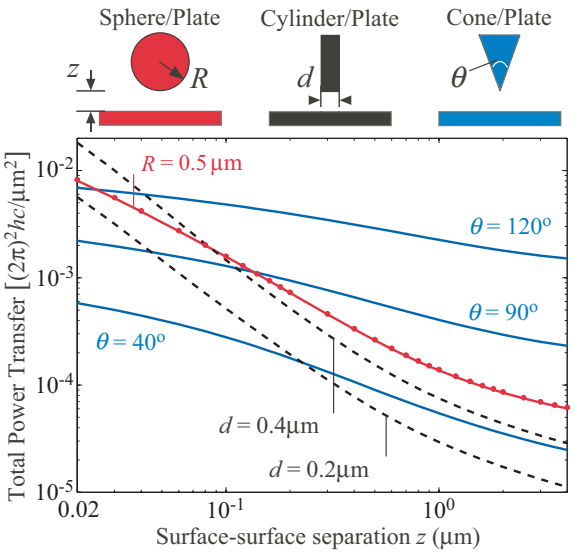

FIG. 1. (Color online) Total thermal transfer between a silica plate and doped silicon objects of various shapes. The plate is semi-infinite, and the objects all have heights equal to 1 μm in the z direction. The plate/environment temperature is $T_P = 300$ K and the objects are at temperature $T_A = 600$ K. Red dots denote results with the sphere scattering matrix determined analytically, the only case in which we have an analytic solution for the scattering matrix.

contribute to the Poynting flux (which is obtained at the end by taking $\lim_{x'\to x}\nabla_{x'}\times\langle\mathbf{E}\otimes\mathbf{E}'^{*}\rangle^{\mathrm{neq}}$) which is expressed as an integral of the general form

$$\langle\mathbf{E}\otimes\mathbf{E}'^{*}\rangle_j^{\mathrm{neq}} = \int_0^\infty \frac{d\omega}{2\pi}\Theta(\omega,T_j)\langle\mathbf{E}\otimes\mathbf{E}'^{*}\rangle_{j,\omega}^{\mathrm{neq}},$$

where $\Theta = \omega^4[\exp(\hbar\omega/k_BT)-1]^{-1}$,[17,18] $\hbar$ is Planck's constant, and k_B is the Boltzmann constant. Unless otherwise noted, we consider each frequency ω separately and drop the ω subscript below.

The correlator takes on a simple form in an orthogonal basis $\mathbf{E}_\alpha(\omega;\mathbf{x})$ for the field degrees of freedom (in our case, these will be cylindrical waves in the $\pm z$ direction), indexed by a (discrete or continuous) index α, and representing the correlator as a matrix $\mathbb{D}$. In matrix notation (with implied summation over repeated indices),

$$\langle\mathbf{E}(\mathbf{x})\otimes\mathbf{E}^{*}(\mathbf{x}')\rangle_j^{\mathrm{neq}} = \left(\mathbb{D}_j\right)_{\alpha',\alpha}\mathbf{E}_{\alpha'}(\mathbf{x})\otimes\mathbf{E}_\alpha^{*}(\mathbf{x}'). \qquad (1)$$

The total relevant nonequilibrium part is given by $\mathbb{D}_{\mathrm{total}} = \mathbb{D}_P + \mathbb{D}_E$, where $\mathbb{D}_{P/E}$ involve sources only from P or E. The correlators $\mathbb{D}_{P/E}$ are obtained from the "unperturbed" correlators $\mathbb{D}^0_{P/E}$; $\mathbb{D}^0_P$ involves the plate sources without A, and $\mathbb{D}^0_E$ involves the environment sources with neither A nor P present. The $\mathbb{D}^0_j$ are known analytically (see below), and the full correlators $\mathbb{D}_j$ can be determined from them by use of the Lippmann-Schwinger equation.[8,19] In our notation,

$$\mathbb{D}_j = \mathbb{O}_j\mathbb{D}^0_j\mathbb{O}_j^\dagger, \quad j = P,E. \qquad (2)$$

The $\mathbb{O}_j$ are matrices that describe the scattering of incoming and outgoing fields with the allowance for sources in between the objects, described explicitly in Ref. 20. These are constructed from the more conventional incoming or outgoing scattering matrices $\mathbb{F}_{P/A}$[19,21] for objects P and A individually. As object P is a plate, $\mathbb{F}_P$ is known analytically. As $\mathbb{F}_A$ cannot be determined analytically for a general object A, the computation of the scattering matrix elements is accomplished via a boundary-element method,[13] described below. The z component of the Poynting flux at position $\mathbf{x}$, $S_{\mathbf{x}}$, and the total power flux S_T through the the surface of P at $z = 0$ can both be expressed as operator traces: $S_{\mathbf{x}/T} = \mathrm{Re}\,\mathrm{Tr}\left[\mathbb{S}_{\mathbf{x}/T}\mathbb{D}_{\mathrm{total}}\right]$, with $(\mathbb{S}_{\mathbf{x}})_{\alpha',\alpha} = -\frac{i}{\omega}\hat{\mathbf{z}}\left\{\mathbf{E}_\alpha(\mathbf{x})\times[\nabla\times\mathbf{E}_{\alpha'}(\mathbf{x})]^*\right\}$ and $(\mathbb{S}_T)_{\alpha',\alpha}$ given below.

We employ a cylindrical wave basis of fields $\mathbf{E}_{s,m,k_\rho,p}(\mathbf{x})$ in which the waves (also known as Bessel beams) propagate in the $\pm z$ direction.[22] The variable $s = \pm$ refers to the direction of propagation; m is the (integer) angular moment of the field, $0 \leqslant k_\rho < \infty$ is the radial wave vector, and $p = M,N$ is the polarization. The composite index in this case is $\alpha = \{s,m,k_\rho,p\}$. This basis is especially well suited to the case considered here in which objects have rotational symmetry about the z axis, as different values of m are decoupled.

To compute the elements of $\mathbb{F}_A$, we use a boundary-element method (BEM).[13,23] In this framework, the surface of object A is discretized into a mesh; our numerical method then computes the induced currents from an incident multipole field $\mathbf{E}_\alpha(\mathbf{x})$; here $\alpha = \{s,m,k_\rho,p\}$. The multipole moments of this current distribution are then computed in a straightforward manner,[22] which yields the scattering matrix $\mathbb{F}_A$.[19] Because the cylindrical wave basis distinguishes between waves in the $\pm z$ direction (unlike a spherical wave basis), and because the near-field thermal transport mostly depends on reflections from adjacent surfaces, we are able to concentrate most of our BEM mesh resolution on the part of A nearest the plate, allowing us to solve problems that are numerically intractable in a spherical wave basis. For example, in the mesh for a cone below we use $\sim$250 times more resolution at the tip than at the base.

One complication of cylindrical multipoles is that k_ρ is a continuous index and matrix multiplication is turned to integration. For computational purposes, this integration must be approximated as a discrete sum by numerical quadrature. We approximate the integral over k_ρ using a Gaussian quadrature scheme[24] for high accuracy. For example, consider the scattering matrix $\mathbb{F}_A$ of object A; its action on an incident electric field can be discretized as (for simplicity, the summation over m and p is suppressed) $\mathbb{F}_A\mathbf{E}_{k_{\rho,i}} = \int_0^\infty \frac{dk'_\rho}{2\pi}(\mathbb{F}_A)_{k'_\rho;k_{\rho,i}}\mathbf{E}_{k'_\rho} \approx \sum_{j=0}^N w_j(\mathbb{F}_A)_{j,i}\mathbf{E}_{k_{\rho,j}}$, where the sets $\{w_j,k_{\rho,j}\}$ form a set of one-dimensional quadrature weights and points, respectively, and $(\mathbb{F}_A)_{j,i} = (\mathbb{F}_A)_{k_{\rho,j},k_{\rho,i}}$ are the elements of the continuous scattering matrix.

The analytic expression for the nonequilibrium electric-field correlator of a plate at temperature T_P and environment at $T = 0$ expressed in the plane-wave basis is well known.[17,20] Transforming plane waves to cylindrical waves, it is a simple exercise to reexpress this correlator in the basis of cylindrical multipoles:[22]

$$\left(\mathbb{D}^0_P\right)_{\alpha',\alpha} = \delta_{\alpha',\alpha}\delta_{s,+}\left(\frac{1-|r_{k_\rho,p}|^2}{4qk_\rho}\chi_p + \frac{\mathrm{Im}\,r_{k_\rho,p}}{2|q|k_\rho}\chi_e\right).$$

Here $r_{k_\rho,p}$ are the Fresnel coefficients for a dielectric plate, $\chi_{p(e)} = 1$ for $k_\rho < \omega$ ($k_\rho > \omega$) and zero otherwise, $q = \sqrt{\omega^2-k_\rho^2}$,

and $\delta_{i,j}$ is the Kronecker (Dirac) delta function on discrete (continuous) indices; the $\delta_{s,+}$ reflects the fact that only waves propagating in the $+z$ direction are emitted by the plate. The expression for the environment correlator $\mathbb{D}_E^0$ is given by the same expression as $\mathbb{D}_P^0$ with $r = 0$ and $\delta_{s,+}$ replaced with $\delta_{s,-}$. Finally, the matrix elements for the total power flux are $(\mathbb{S}_T)_{\alpha',\alpha} = \frac{2\pi q k_\rho}{\omega}\delta_{k_\rho,k'_\rho}\delta_{p,p'}(-s')^{\delta_{p',N}}[(\chi_p - \chi_e)s]^{\delta_{p,M}}$.

For the surface meshes, we use approximately 2500 panels (discretized surface elements) to get 1% convergence for the total power transfer, with the panels highly concentrated on the area of the objects nearest to the plate. For the spatially resolved heat flux, we will require more fine meshes of 12 000 panels for the cones (see below). In spherical coordinates, there is a distinction between polar (ℓ) and azimuthal moments m; for our semianalytic sphere-plate calculations, we require ℓ up to 60. However, far fewer m are required (due to rotational symmetry), and we require only azimuthal moments up to $|m| = 10$ for 1% accuracy. For each m we perform the ω and k_ρ integrations using 28 and 48 Gaussian quadrature points, respectively. For our study, object A is composed of doped silicon while the substrate B is silica. For the doped silicon dispersion we use a standard Drude-Lorentz model[25] with a dopant density of $1.4 \times 10^{19}\text{cm}^{-3}$, while for silica we use measured optical data.[3]

III. RESULTS

Figure 1 shows the geometry dependence of the total heat transfer rate between different compact objects and a dielectric plate, over surface-surface separations z from several microns down to 20 nm. In addition to the expected near-field enhancement, we observe several crossings as, e.g., the broader surface area of the $R = 0.5$-μm-radius sphere competes with the smaller but flatter surface of the $d = 0.4$-μm-diameter cylinder. For smaller z, the ratio of the transfer between the $d = 0.4$- and 0.2-μm cylinders approaches the ratio of their surface areas (within 6% at $z = 20$ nm), as would be expected from a proximity approximation (PA).[7,8] The sphere-plate exhibits the $1/z$ power law as predicted by PA[3,4,8] to within 10% for $z < 0.1\,\mu$m, while the cylinder-plate exhibits agreement to within approximately 10% over this range using a PA based on the integral of the plate-plate heat transfer rate over the cylinder front face and vertical sidewalls. The contribution from the sidewalls can be ignored (leading to a $\sim 1/z^2$ transfer rate)[6] for $z/d \lesssim 0.01$. In contrast to the sphere and cylinders, the cones have a *logarithmic* divergence as $z \to 0$, which results from the scale invariance of the plate-cone configuration when $z \ll 1\,\mu$m and $\hbar c/k_B T$ (the latter eliminating material-dispersion effects).[26] To check the accuracy of our numerical scattering method, we also plot the results for the sphere where $\mathbb{F}_A$ is calculated semianalytically,[8] shown as red dots, which agrees to within 1%.

For thermal writing applications, an important factor to consider is not only the total power delivered to the plate but also the spatial extent over which this delivery occurs. In order to examine this, we envision a scenario in which a critical magnitude of the z-directed Poynting flux is required in order for some change to occur on the plate, for example, the patterning of a thermal mask for later etching.[2] Figure 2 plots the Poynting flux at $x = 0$ as a function of z, which will

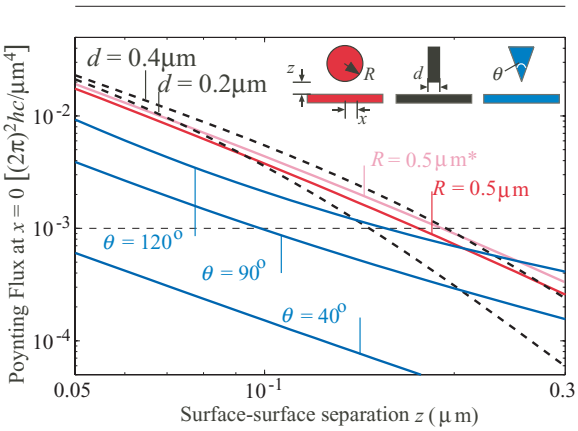

FIG. 2. (Color online) Poynting flux at the origin for the geometries of Fig. 1 with plate/environment temperature $T_P = 300$ K and object temperature $T_A = 600$ K, using the single polarization approximation (SPA) for the sphere and cylinders. The light pink line denotes the sphere-plate without the SPA, and the horizontal dashed line denotes the threshold used for the cross-sectional flux profiles of Fig. 3.

tell us how close the object must be before it can effect this patterning. The cylinders and spheres converge to the same $\sim 1/z^2$ profile for small z (as expected from a PA), whereas the cones all follow $1/z^2$ profiles with different coefficients. This $1/z^2$ dependence follows from the scale invariance of the scattering problem for small z, combined with the fact that there is a $1/z$ cutoff in the range of k_ρ that contributes to the transfer, so that the total number of modes that contribute is proportional to $\int_0^{1/z} dk_\rho k_\rho \sim 1/z^2$. In this calculation we have found that the results for spheres and cylinders are dominated by the N polarization ($\mathbf{E} \perp \hat{\mathbf{z}}$), mirroring similar phenomena in other near-field cases,[27] that results from the behavior of the Fresnel coefficients for high k_ρ. This is fortunate because we have found that the M contribution to the Poynting flux requires much higher mesh resolution to converge; although we achieve this for cones by switching to a mesh of 12 000 panels, this resolution is intractable for spheres and cylinders, so for computing the spatially resolved Poynting vector in the latter cases we use the single polarization approximation

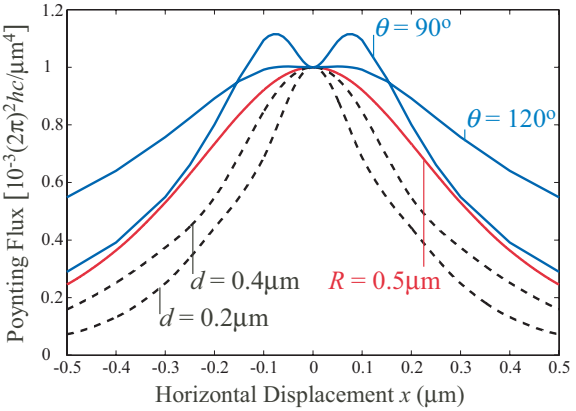

FIG. 3. (Color online) Spatially resolved heat flux profiles at the substrate surface. z is chosen to fix the Poynting flux at $x = 0$ at $10^{-3}(2\pi)^2 hc/\mu\text{m}^4$.

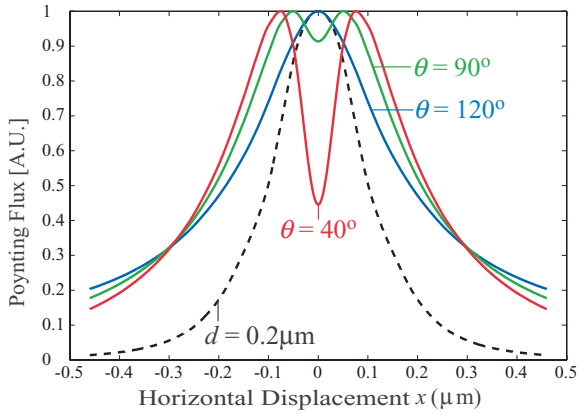

FIG. 4. (Color online) Spatially resolved heat flux profiles (arbitrary units) at the substrate surface for all three cones at $z = 70$ nm. The profiles are normalized so that their maximal value is equal to one. For comparison, the profile for a cylinder of radius $d = 200$ nm (using the SPA) is shown as well.

(SPA) of neglecting the M contributions. We check the SPA for a sphere by plotting the full results in Fig. 2, finding that the error from the SPA is $<20\%$ at the largest z, decaying to $<10\%$ at smaller z.

Figure 3 plots the Poynting flux as a function of x showing the heat transfer profile. For each object, we chose z to have the same $x = 0$ Poynting flux of $10^{-3}(2\pi)^2 hc/\mu\text{m}^4$ (the horizontal dashed line in Fig. 2), corresponding to a sphere-plate separation of $\approx$200 nm. The cylinders and 120° cone all reach this threshold at comparable separations, whereas the 90° cone is at less than half the separation, and the 40° cone does not even reach this threshold within the range considered.

Fixing the peak Poynting flux to $10^{-3}(2\pi)^2 hc/\mu\text{m}$,[4] in Fig. 3 we plot the Poynting flux profiles for these shapes as a function of x. The widths for the cylinders are narrower than the sphere, implying that the cylinders can write higher spatial resolution. Surprisingly, the cones do not exhibit this simple behavior. Rather, the Poynting flux profiles for the two cones are *non*monotonic in x, with a local minimum at $x = 0$. The degree of nonmonotonicity appears to increase as the cone becomes sharper.

To confirm this, we plot the Poynting flux for all three cones in Fig. 4 at a fixed $z = 70$ nm; for ease of comparison, all curves are scaled to have a maximum of one. We also show the $d = 200$-nm cylinder (using the SPA) for comparison. The relative strength of the dip at $x = 0$ increases as θ decreases, approaching half the maximum at $\theta = 40°$. It is interesting to note that this effect allows a sharp cone to write *rings* rather than spot profiles, and that these rings can be as finely resolved as the spots for a cylinder. We believe the explanation for the dip in the Poynting flux is that, as the cone tip becomes sharper, its radiation pattern approaches that of a point dipole with the axis normal to the plate, which has zero Poynting flux at $x = 0$. This explanation predicts that a very thin cylinder with $d \ll z$ should also have a dip in the Poynting flux at $x = 0$, which we have confirmed numerically (without approximation). This may also have implications for surface roughness, where the many tiplike features in a roughened surface could lead to results that differ qualitatively from PA predictions.

ACKNOWLEDGMENTS

This work was supported by the Army Research Office through the Institute for Soldier Nanotechnologies under Contract No. W911NF-07-D-0004, by the Defense Advanced Research Project Agency under Contract No. N66001-09-1-2070-DOD, and by the Deutsche Forschungsgemeinschaft under Grant No. KR 3844/1-1.

[1] H. J. Mamin, Appl. Phys. Lett. **69**, 433 (1996).
[2] K. Wilder, C. F. Quate, D. Adderton, R. Bernstein, and V. Elings, Appl. Phys. Lett. **73**, 2527 (1998).
[3] S. Shen, A. Narayanaswamy, and G. Chen, Nano Lett. **9**, 2909 (2009).
[4] E. Rousseau, A. Siria, G. Jourdan, S. Volz, F. Comin, J. Chevrier, and J.-J. Greffet, Nature Photonics **3**, 514 (2009).
[5] D. Polder and M. Van Hove, Phys. Rev. B **4**, 3303 (1971).
[6] A. I. Volokitin and B. N. J. Persson, Phys. Rev. B **63**, 205404 (2001).
[7] A. Narayanaswamy and G. Chen, Phys. Rev. B **77**, 075125 (2008).
[8] M. Krüger, T. Emig, and M. Kardar, Phys. Rev. Lett. **106**, 210404 (2011).
[9] C. Otey and S. Fan, Phys. Rev. B **84**, 245431 (2011).
[10] G. Bimonte, Phys. Rev. A **80**, 042102 (2009).
[11] R. Messina and M. Antezza, Euro. Phys. Lett. **95**, 61002 (2011).
[12] A. W. Rodriguez, O. Ilic, P. Bermel, I. Celanovic, J. D. Joannopoulos, M. Soljačić, and S. G. Johnson, Phys. Rev. Lett. **107**, 114302 (2011).
[13] S. Rao, D. Wilton, and A. Glisson, IEEE Trans. Anten. Prop. **30**, 409 (1982).
[14] J. B. Pendry, J. Phys. Condens. Matter **11**, 6621 (1999).
[15] A. I. Volokitin and B. N. J. Persson, Rev. Mod. Phys. **79**, 1291 (2007).
[16] J. P. Mulet, K. Joulain, R. Carminati, and J. J. Greffet, Appl. Phys. Lett. **78**, 2931 (2001).
[17] S. M. Rytov, Y. A. Kravtsov, and V. I. Tatarskii, *Principles of Statistical Radiophysics III* (Springer-Verlag, New York, 1989).
[18] W. Eckhardt, Phys. Rev. A **29**, 1991 (1984).
[19] S. J. Rahi, T. Emig, N. Graham, R. L. Jaffe, and M. Kardar, Phys. Rev. D **80**, 085021 (2009).
[20] M. Krüger, T. Emig, G. Bimonte, and M. Kardar (unpublished).
[21] E. Merzbacher, *Quantum Mechanics* (Wiley, New York, 1998).
[22] L. Tsang, J. A. Kong, and K.-H. Ding, *Scattering of Electromagnetic Waves* (Wiley, New York, 2000).
[23] M. T. H. Reid, Ph.D. thesis, Massachusetts Institute of Technology, 2010.
[24] M. Abramowitz and I. A. Stegun, *Handbook of Mathematical Functions* (Dover, New York, 1972).
[25] L. Duraffourg and P. Andreucci, Phys. Lett. A **359**, 406 (2006).
[26] A. P. McCauley, Ph.D. thesis, Massachusetts Institute of Technology, 2011.
[27] Z. M. Zhang, *Nano/Microscale Heat Transfer* (McGraw-Hill, New York, 2007).